NANOMATERIALS

# Polymer ligand–induced autonomous sorting and reversible phase separation in binary particle blends

Michael Schmitt,[1]* Jianan Zhang,[1,2]*† Jaejun Lee,[1] Bongjoon Lee,[1] Xin Ning,[1]‡ Ren Zhang,[3] Alamgir Karim,[3] Robert F. Davis,[1] Krzysztof Matyjaszewski,[2]§ Michael R. Bockstaller[1]§



**The tethering of ligands to nanoparticles has emerged as an important strategy to control interactions and organization in particle assembly structures. We demonstrate that ligand interactions in mixtures of polymer-tethered nanoparticles (which are modified with distinct types of polymer chains) can impart upper or lower critical solution temperature (UCST/LCST)–type phase behavior on binary particle mixtures in analogy to the phase behavior of the corresponding linear polymer blends. Therefore, cooling (or heating) of polymer-tethered particle blends with appropriate architecture to temperatures below (or above) the UCST (or LCST) results in the organization of the individual particle constituents into monotype microdomain structures. The shape (bicontinuous or island-type) and lengthscale of particle microdomains can be tuned by variation of the composition and thermal process conditions. Thermal cycling of LCST particle brush blends through the critical temperature enables the reversible growth and dissolution of monoparticle domain structures. The ability to autonomously and reversibly organize multicomponent particle mixtures into monotype microdomain structures could enable transformative advances in the high-throughput fabrication of solid films with tailored and mutable structures and properties that play an important role in a range of nanoparticle-based material technologies.**

## INTRODUCTION

The unique physical properties of nanocrystalline materials with controlled size and shape have rendered inorganic nanocrystals and their assembly structures an important platform to facilitate technological breakthroughs in areas ranging from sustainable energy technologies to magnetic storage or medical diagnostics (*1*–*3*). A widely used approach to integrate particle-based materials into device structures relies on the fabrication of films from particle dispersions (*3*). The process of structure formation in particle thin or thick films (hereafter referred to as "particle solids") has thus been the subject of intense research (*4*–*8*). Driven by the advancement of synthetic and particle size separation techniques as well as the understanding of the physics underlying the organization of colloidal systems, the controlled assembly of one- and two-component particle systems into uniform long-ranged ordered structures that mimic atomic crystal structures has been achieved (*9*). To augment the structure and properties of particle solids, the tethering of organic ligands to the surface of particles has emerged as an effective strategy. This approach takes advantage of the possibility to tailor the interactions between particle constituents by the deliberate design of the structure and composition of organic ligands. For example, Shevchenko and coworkers (*9*) demonstrated that the variation of aliphatic ligands in binary particle mixtures enables the controlled assembly of a range of binary particle superlattice structures. The tethering of DNA-based ligands that are capable of directional interactions was shown to be an effective method to assemble particles into a range of open lattice structures (*10*, *11*).

Recent advances in surface-initiated controlled radical polymerization have further extended the range of possible ligand compositions to encompass polymer chains (*12*). Properties of materials assembled from polymer-tethered particles were shown to sensitively depend on the grafting density and degree of polymerization of tethered chains as well as the size and geometry of the particle core (*12*). For the special case of densely polymer-tethered particle systems (hereafter referred to as "particle brushes"), it was shown that increasing the chain length of ligands gives rise to a transition from hard sphere–type to soft interactions and a progressively more polymer-like response of particle solids (*13*). The tailoring of brush architectures has been shown to offer intriguing opportunities to augment the properties of particle solids. For example, polymer ligands were shown to increase the elastic modulus and toughness of colloidal crystal-type particle solids, to enable their processing by solventless molding techniques, and to facilitate hybrid materials with enhanced dielectric and novel phononic properties (*14*–*19*).

Beyond the enhancement of mechanical properties, the macromolecular nature of polymers gives rise to unique physicochemical characteristics that could enable transformative advances in the development of high-throughput fabrication techniques of microstructured particle solid films. Here, we demonstrate that polymer-ligand interactions can induce upper or lower critical solution phase behavior in multicomponent particle solids depending on the polymer ligand composition. Hence, cooling (or heating) of particle brush blends with appropriate architecture below (or above) the upper (or lower) critical solution temperature (UCST/LCST) of the blend results in the formation of monotype particle microdomains with characteristic lengthscales that can be tuned by adjustment of the thermal annealing conditions. Thermal cycling of LCST particle brush blends at temperatures above and below the critical temperature enables the reversible growth or shrinkage of monoparticle domain structures. This process could ultimately facilitate the reversible formation and dissolution of microstructures in multicomponent particle solids. Figure 1 illustrates the process

[1]Department of Materials Science and Engineering, Carnegie Mellon University, 5000 Forbes Avenue, Pittsburgh, PA 15213, USA. [2]Chemistry Department, Carnegie Mellon University, 4400 Fifth Avenue, Pittsburgh, PA 15213, USA. [3]Department of Polymer Engineering, Polymer Engineering Academic Center, University of Akron, 250 South Forge Street, Akron, OH 44325–0301, USA.
*These authors contributed equally to this work.
†Present address: School of Chemistry and Chemical Engineering, Anhui University, 111 Jiulong Road, Hefei 230601, China.
‡Present address: Department of Materials Science and Engineering, Rensselaer Polytechnic Institute, 110 Eighth Street, Troy, NY 12180, USA.
§Corresponding author. Email: bockstaller@cmu.edu (M.R.B.); km3b@andrew.cmu.edu (K.M.)

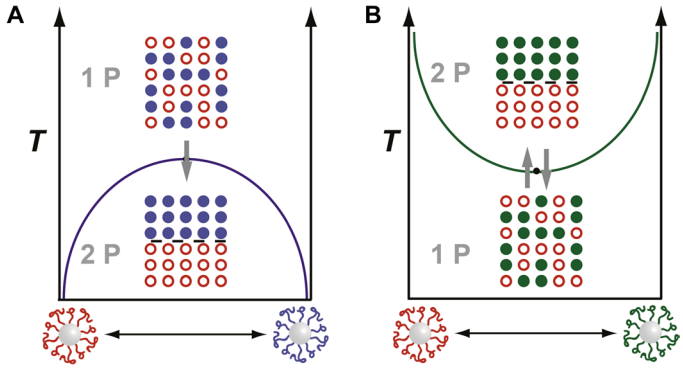


**Fig. 1. Illustration of ligand-induced phase separation in particle brush blends.** (**A**) UCST phase behavior. (**B**) LCST phase behavior. LCST blends allow for reversible cycling of blend through homogeneous one-phase (1 P) and phase-separated two-phase (2 P) states.

for controlled organization in binary particle brush mixtures by harnessing polymer ligand–induced phase transitions.

## RESULTS

The binary blend systems in our study consist of silica particles (average radius $R_0$ = 7.7 ± 2 nm and $R_0$ = 60.3 ± 4 nm) tethered with poly(methyl methacrylate) (PMMA), polystyrene (PS), or poly(styrene-*r*-acrylonitrile) (PSAN) ligands. The tethered polymers are amorphous and exhibit high glass transition temperatures (that is, $T_{g,PS} \approx 110$°C, $T_{g,PMMA} \approx 105$°C, and $T_{g,PSAN} \approx 118$°C), which enable the rapid vitrification of blend films for subsequent structural analysis. PS/PMMA ligands were chosen because the corresponding linear polymers present a widely studied prototype system for UCST polymer blends (*20*). The Flory-Huggins interaction parameter for PS/PMMA is $\chi_{S/MMA} = 0.028 + 3.9/T$, where $T$ is the absolute temperature (*21*). Because of the strong repulsive interaction between repeat units and the low ceiling temperature of PMMA ($T_{ceil} \approx 220$°C), miscibility in linear PS/PMMA blends (at $T >$ UCST) can only be observed for low–molecular weight systems (*20*). As will be shown below, this precludes the possibility to accomplish reversible phase separation and dissolution in $SiO_2$-PS/$SiO_2$-PMMA particle brush blends. In contrast, PMMA/PSAN constitutes a miscible polymer blend with LCST behavior that shows a reversible transition between miscible and phase-separated states provided that the molar ratio $\nu = n(AN)/n(S)$ is within the miscibility window $0.09 < \nu < 0.38$ (*22*). The interaction parameter of the PSAN/PMMA system depends on both the constitution of PSAN as well as the composition of the blend. Here, the molar composition of the random copolymer is S/AN = 3:1—the corresponding interaction parameter is $\chi_{MMA/SAN} \approx -0.15$ (at $T \approx$ 25°C). The LCST of linear PMMA/PSAN blends is approximately 160°C for a polymer molecular weight of $M_w \approx 90{,}000$ (*23*, *24*).

Particle brush systems were synthesized by surface-initiated atom transfer radical polymerization (SI-ATRP) following previously published procedures (*25*–*27*). To avoid cross-linking of polymer tethers during prolonged thermal annealing, we debrominated samples after synthesis (see Materials and Methods). Silica particles were chosen as model systems, primarily because the strong covalent coupling of polymer tethers facilitates stable ligand bonds up to $T \approx 250$°C (as evidenced by thermogravimetric analysis, not shown here). To enable the analysis of structure evolution on practical time scales, we chose the average particle size to be $R_0$ = 7.7 ± 2 nm; however, for select systems, a particle size of $R_0$ = 60.3 ± 4 nm was tested to evaluate the role of particle size in ligand-induced phase separation. In total, 10 types of particle brush systems were synthesized to elucidate the effect of composition and degree of polymerization of ligands on the phase separation of particle brush blends. The grafting density was approximately $\sigma_S \approx 0.5$ nm$^{-2}$ for all particle brush systems, which is consistent with dense grafting. The molecular characteristics of all particle brush systems along with the respective sample IDs are summarized in Table 1.

**Table 1. Summary of molecular characteristics of particle brush systems.** Sample IDs reflect sample characteristics where the first number indicates the approximate particle radius in nanometers. S, styrene; MMA, methyl methacrylate; SAN, styrene-*r*-acrylonitrile with (S/AN) = 3:1 graft composition. $N$ is the degree of polymerization of surface grafted chains, $M_{n,\,GPC}$ is the number average molecular weight as determined by gel permeation chromatography (GPC), $M_w/M_n$ is the molecular weight dispersity, and $\theta_s$ is the surface grafting density. wt %, weight percent.

| Sample ID | $N$ | $M_{n,\,GPC}$ | $M_w/M_n$ | $\theta_s$ (nm$^{-2}$) | $SiO_2$ wt % |
|---|---|---|---|---|---|
| 8$SiO_2$-S62 | 62 | 6,500 | 1.22 | 0.76 | 56 |
| 8$SiO_2$-S205 | 205 | 21,400 | 1.36 | 0.49 | 22 |
| 8$SiO_2$-S360 | 360 | 37,900 | 1.14 | 0.64 | 14 |
| 60$SiO_2$-S1300 | 1300 | 135,200 | 1.29 | 0.59 | 25 |
| 8$SiO_2$-MMA68 | 68 | 6,800 | 1.30 | 0.41 | 58 |
| 8$SiO_2$-MMA194 | 194 | 19,400 | 1.17 | 0.65 | 25 |
| 8$SiO_2$-MMA257 | 257 | 25,700 | 1.32 | 0.49 | 21 |
| 8$SiO_2$-MMA350 | 350 | 35,000 | 1.12 | 0.56 | 13 |
| 60$SiO_2$-MMA1470 | 1470 | 147,000 | 1.18 | 0.93 | 16 |
| 8$SiO_2$-SAN262 | 262 | 22,300 | 1.15 | 0.64 | 19 |

Particle brush blend films with thickness of 110 to 140 nm (corresponding approximately to five to eight particle layers) were prepared by spin casting from tetrahydrofuran (THF) solution onto ⟨100⟩ silicon substrates with a native oxide layer and subsequently vacuum-annealed for up to 7 days. Films were smooth and contiguous; the absence of cross-linking was confirmed by film dissolution tests and infrared (FTIR) vibration spectroscopy. The surface morphology was investigated using atomic force microscopy (AFM) driven in tapping mode. For each sample, several scans over distinct sample areas of 25 μm$^2$ were conducted to ensure consistency. Because established processes to etch PMMA or PS domains (for example, by exposing samples to ultraviolet/ozone and subsequent immersion in acetic acid for PMMA or by immersion in cyclohexane for PS) were not successful, transmission electron microscopy (TEM) was performed on select samples to identify the composition of phases. For electron imaging analysis, ⟨100⟩ silicon substrates were precoated with a thin (≈50 nm) film of poly(acrylic acid) (PAA) before film deposition. Films were transferred to TEM grids after thermal annealing by immersion into water (we note that films of the low molecular 8$SiO_2$-MMA68/8$SiO_2$-S62 blend system could not be processed in this way because of the brittle nature of the films). The characteristic domain sizes of phase-separated particle brush films were determined from AFM or TEM images using the line intersection method. Fast Fourier transform analysis (a frequently used method to determine

correlation lengths) could not be applied in the present case because of the interference of the particle cores with the required image thresholding.

We first discuss the results on the $8SiO_2$-PS/$8SiO_2$-PMMA particle brush systems with UCST phase behavior. Figure 2 depicts representative AFM phase images of symmetric molecular weight binary blends of $8SiO_2$-MMA194/$8SiO_2$-S205 at varying compositions: MMA/S = 25:75 (Fig. 2, A and B), 50:50 (Fig. 2, C and D), and 75:25 (Fig. 2, E and F) after $t$ = 48 hours of thermal annealing at $T$ = 200°C (Fig. 2, A, C, and E), 160°C (Fig. 2D), and 140°C (Fig. 2, B and F). The micrographs reveal a transition from discrete island-type morphology, indicative of phase separation by nucleation and growth (NG) for asymmetric blend compositions to bicontinuous network–type structures, indicative of phase separation initiated by spinodal decomposition (SD) for symmetric blend compositions. The observed structural transitions show similarity to previous reports on phase-separated structures of linear PS/PMMA polymer blend systems—this is illustrated in Fig. 2G, which compiles the observed microstructures within a UCST phase diagram that was calculated for a PS/PMMA ($N_{PS}$ = 205 and 194) reference system using the Flory-Huggins theory (*20*). It should be noted that the depiction of a bulk-type UCST phase diagram (Fig. 2G) serves to only illustrate the conceptual similarity between the observed morphologies in the $8SiO_2$-MMA194/$8SiO_2$-S205 systems and the expected behavior for binary linear polymer blends. The influence of geometric confinement, polymer tethering, and substrate interactions on structure evolution during phase separation is not considered in Fig. 2G (*28*, *29*). Nevertheless, the microstructures depicted in Fig. 2 (A to F) reveal remarkable agreement with the expected structure evolution in the unstable (SD) and metastable (NG) compositional range.

To identify phase compositions, we performed electron imaging of select material systems. Figure 3 depicts AFM and TEM images of $8SiO_2$-MMA194/$8SiO_2$-S205 (50:50) at $t$ = 0 and 24 hours of thermal annealing at $T$ = 140°C. In TEM images, PS appears as a dark domain due to ruthenium tetroxide ($RuO_4$) stain. The figure reveals that as-spun films are approximately homogeneous (Fig. 3, A and C), whereas a bicontinuous network structure is observed after thermal

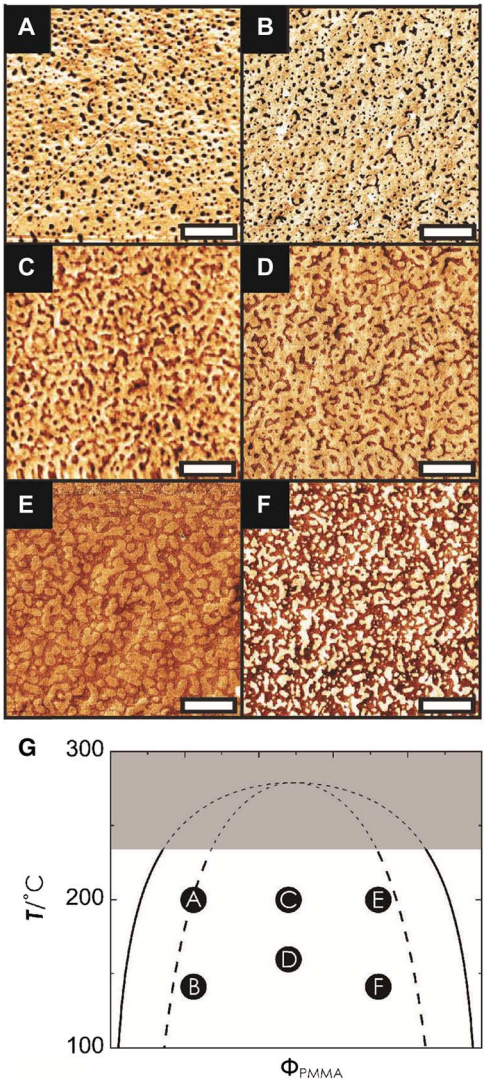


**Fig. 2. Phase separation in $8SiO_2$-MMA194/$8SiO_2$-S205.** AFM phase images of film morphologies at varying composition and annealing temperature after $t$ = 48 hours of thermal annealing. Dark phase corresponds to PMMA. (**A**) PMMA/PS = 25:75; $T$ = 200°C. (**B**) PMMA/PS = 25:75; $T$ = 140°C. (**C**) PMMA/PS = 50:50; $T$ = 200°C. (**D**) PMMA/PS = 50:50; $T$ = 160°C. (**E**) PMMA/PS = 75:25; $T$ = 200°C. (**F**) PMMA/PS = 75:25; $T$ = 140°C. (**G**) UCST phase diagram for a reference PS/PMMA homopolymer blend with $N_{PS}$ = 205 and $N_{PS}$ = 194 calculated using Flory-Huggins theory (see text for more details). Solid line, binodal; dotted line, spinodal. The region enclosed by the spinodal marks the "unstable regime" where separation by SD is expected. Region highlighted in gray is not accessible to experiments due to thermal degradation of PMMA. Scale bars in (A) to (F), 1 micron.

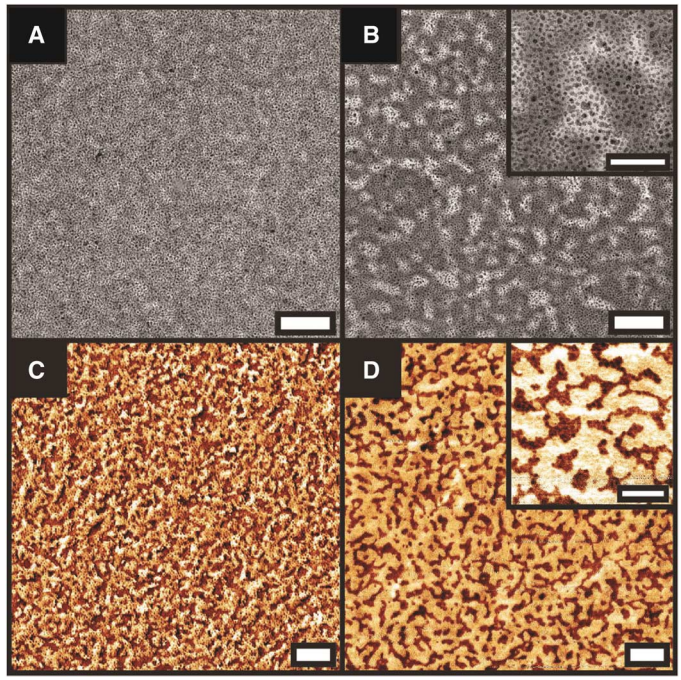


**Fig. 3. Structure characterization of films before and after thermal annealing.** Images show structure evolution in a symmetric blend of $8SiO_2$-MMA194/$8SiO_2$-S205 (50:50). (**A**) Bright-field TEM image after thermal annealing at $T$ = 140°C for $t$ = 0. (**B**) Bright-field TEM image after thermal annealing at $T$ = 140°C for $t$ = 24 hours. (**C**) AFM phase image after thermal annealing at $T$ = 140°C for $t$ = 0. (**D**) AFM phase image after thermal annealing at $T$ = 140°C for $t$ = 24 hours. Insets in (B) and (D) show magnified view of the phase-separated structure. PS domain appears dark in (A) and (B) ($RuO_4$ stain); PS domain appears bright in (C) and (D). Electron micrographs further reveal uniform distribution of particle centers (small dark dots) thus confirming uniform film structure before and after thermal annealing. Scale bars, 500 nm (main figures) and 250 nm (insets).

annealing for 24 hours (Fig. 3, B and D). It is noted that electron images of as-spun films (such as Fig. 3A) reveal a shallow contrast variation that bears similarity to phase-separated morphologies—an indication that phase separation commences already during the film fabrication process.

Analysis of the areal fraction of the respective phases in the AFM and TEM images (for asymmetric blend compositions, not shown here) reveals that PMMA appears as a darker domain in scanning probe images. Note that the uniform distribution of particle cores in electron images (Fig. 3, A and B) confirms the contiguity as well as the approximately constant thickness of films because undulations of film thickness across the imaged area would result in fluctuations of the particle density in projection electron images.

The uniform film thickness is confirmed by concurrent AFM height and phase image analysis shown in Fig. 4 for the case of $8SiO_2$-MMA194/$8SiO_2$-S205 (50:50) after 24 hours of thermal annealing at $T$ = 140°C. The figure illustrates long wavelength height fluctuations with amplitude of about 15 nm (approximately equal to one particle brush diameter that is estimated to be ≈21 nm based on TEM analysis) across areas of the order of 1 $\mu m^2$. This might be interpreted as terrace formation of particle films, possibly due to surface tension variations of the phases. No systematic growth of long wavelength fluctuations was observed during continued annealing. This may be due to pinning of phase separation that typically occurs in thin films from finite size effects. Within terraces, height undulations of about 3 nm were observed on a lengthscale that corresponds to the size of individual domains; maxima correspond to PS and minima to PMMA domains (inferred by correlation of height and phase images). We hypothesize that similar to PS/PMMA linear polymer blends, PS particle brushes "stretch" toward the air/film interface due to the lower surface energy of the PS (that is, $\gamma_{PS}$ = 40.7 mJ/$m^2$ as compared to $\gamma_{PMMA}$ = 41.1 mJ/$m^2$, where $\gamma_i$ denotes the bulk surface tension of component $i$) (*20*, *30*).

To further interrogate the mechanism of phase separation, we analyzed the kinetics of domain growth. Figure 5 depicts the domain growth kinetics for the $8SiO_2$-MMA194/$8SiO_2$-S205 (50:50) blend system annealed at $T$ = 140°C. Analysis of the data in terms of a scaling relation $d \sim t^x$ reveals that the bicontinuous morphology evolves with a scaling coefficient of $x \approx 0.22$ (see Fig. 5A). The fraction of exposed surface coverage of $8SiO_2$-MMA194 (determined from analysis of AFM phase images) is $f_a \approx 0.45$ and independent of the thermal annealing time. The observed depletion of PMMA brushes from the air/film interface is consistent with previous reports on the morphology of PS/PMMA thin films on Si/$SiO_2$ substrates and is attributed to the preferential wetting of the silica by PMMA (*20*).

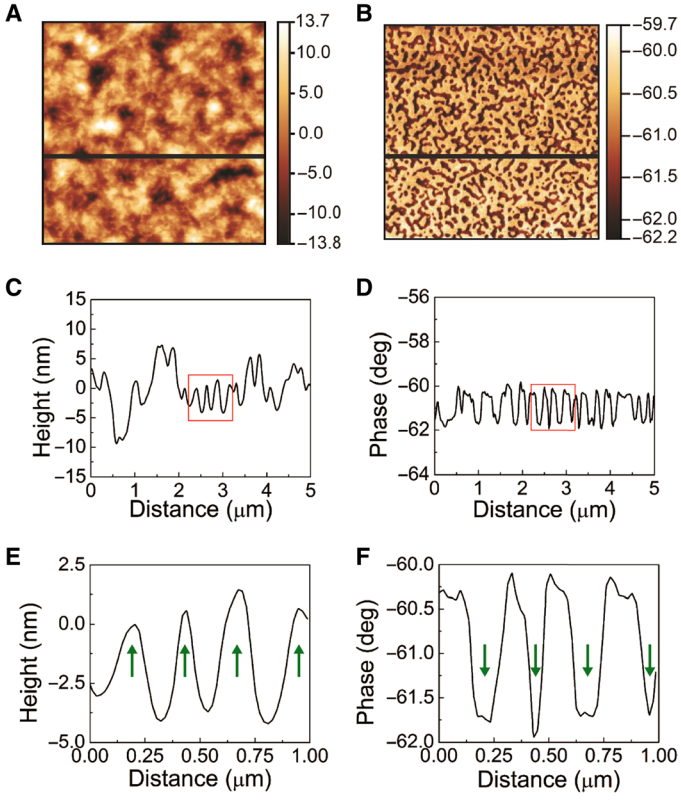


**Fig. 4. Structure and topology of phase-separated films.** (**A**) AFM height image of $8SiO_2$-MMA194/$8SiO_2$-S205 (50:50) after 24 hours of thermal annealing at $T$ = 140°C. (**B**) AFM phase image of same film. $Z$ scale in (A) is in nanometers, $z$ scale in (B) is in degrees. Image size in (A) and (B) is 5 μm; black lines indicate position used for line scans in (**C**) to (**E**). (C) Line scan of height image depicting long wavelength corrugations with amplitude ≈15 nm that occur on the scale of 1 to 2 μm. Red box (C and D) depicts short wavelength corrugations with amplitude ≈3 nm that coincide with domain positions. (E and **F**) Enlarged scans. Maxima in height images correspond to PS and minima to PMMA constituent; for phase images, the PS domain corresponds to minima positions (indicated by green arrows).

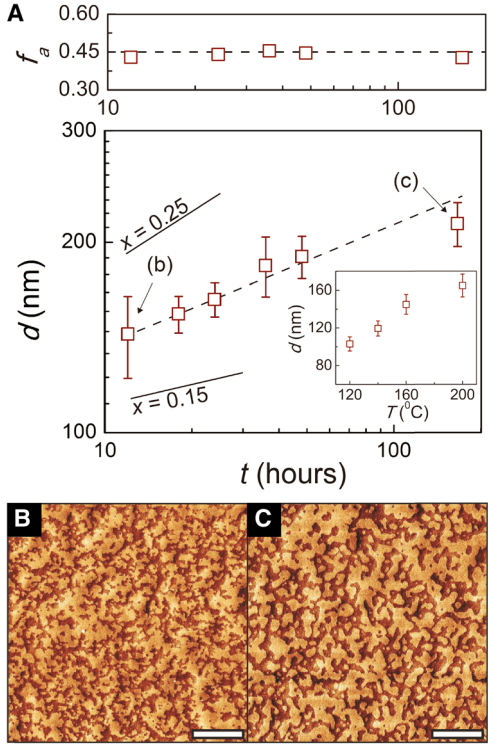


**Fig. 5. Analysis of domain growth kinetics.** (**A**) Characteristic distance $d$ of $8SiO_2$-MMA194/$8SiO_2$-S205 (50:50) blend system during thermal annealing at $T$ = 140°C as a function of annealing time, $t$, revealing the scaling relation $d \sim t^{0.22}$. The areal fraction of PMMA is $f_a$ = 0.45 and independent of annealing time (error bars are within the symbol size). Inset of main figure shows the dependence of $d$ on annealing temperature for a constant annealing time of $t$ = 24 hours. (**B**) AFM phase image of film at $t$ = 12 hours. (**C**) AFM phase image of film at $t$ = 166 hours. Scale bars, 1 μm.

The reduction of $f_a$ by approximately 5% suggests the formation of a monolayer of $8SiO_2$-MMA194 at the silica substrate/particle brush interface. The increase of domain size with annealing temperature (shown in inset of Fig. 5A) is anticipated because the dynamical processes underlying the phase evolution process accelerate with increasing temperature.

To illustrate the role of the size and degree of polymerization $N$ of polymer ligands in the phase separation characteristics of binary particle brush blends, the microstructure formations in symmetric blends of $8SiO_2$-MMA68/$8SiO_2$-S62, $8SiO_2$-MMA194/$8SiO_2$-S205, and $8SiO_2$-MMA350/$8SiO_2$-S360 after 1 week of thermal annealing at $T$ = 140°C are compared in Fig. 6 (insets in Fig. 6 show the structures of the corresponding films before thermal annealing). The figure reveals that phase separation in particle brush blends requires a threshold degree of polymerization as can be inferred from the absence of any discernible phase separation in the $8SiO_2$-MMA68/$8SiO_2$-S62 system. The characteristic domain size of the $8SiO_2$-MMA194/$8SiO_2$-S205 system is larger than the domain size for the longer-chain $8SiO_2$-MMA350/$8SiO_2$-S360 system (218 nm versus 167 nm). This is surprising because the thermodynamic force driving the phase separation process is expected to increase with the degree of polymerization of tethered chains. Both observations point to a pronounced influence of the degree of polymerization of tethered chains on the balance between thermodynamic and dynamical characteristics of particle brush blends (see Discussion).

Note that $N$ also affects the structure of films in the preannealed state. In particular, AFM phase images of the long-chain system $8SiO_2$-MMA350/$8SiO_2$-S360 before annealing reveal a partially phase-separated structure that resembles the morphology of the annealed system (see inset in Fig. 6C). An analogous behavior (albeit less pronounced) is observed in the case of $8SiO_2$-MMA194/$8SiO_2$-S205 (see inset in Fig. 6B). Therefore, phase separation commences already during the vitrification of the film—similar observations have been reported for linear polymer blends with UCST behavior for which it is generally difficult to generate fully homogenized initial states (*20*). To test whether ligand interactions can drive phase separation also in cases of larger colloidal systems, the microstructure formation of a symmetric blend of $60SiO_2$-MMA1470/$60SiO_2$-S1300 was evaluated after 24 hours of thermal annealing at $T$ = 140°C. No phase separation was observed in the pristine blend system (not shown here); however, the addition of 15% of dimethylphthalate (DMP) resulted in the formation of bicontinuous type structures similar to small particle brush analogs as revealed in Fig. 7. This demonstrates both the role of particle brush size and architecture in the kinetics of the separation process (see Discussion) as well as the versatility of ligand-induced phase separation as a method to control the microstructure of multicomponent colloidal assemblies.

In contrast to UCST systems, LCST blends are miscible at low temperatures and phase separate only when temperature is raised above the LCST. LCST polymer blends have attracted much interest as model systems in the study of polymer phase separation because of the better control of the separation process and the possibility to reversibly cycle systems between mixed and phase-separated states by subsequent heating and cooling through the LCST. For mixed particle brush materials, the prospect of reversible phase separation is particularly interesting because it promises intriguing new opportunities to dynamically control the structure (and hence properties) of particle solids. To demonstrate LCST behavior and to test the feasibility

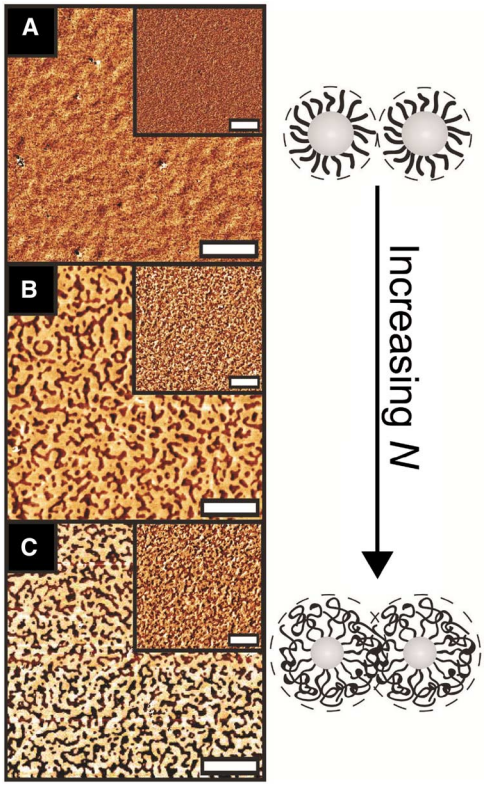


**Fig. 6. Structure formation depends on degree of polymerization of tethered chains.** AFM phase images of symmetric blends $8SiO_2$-MMA68/$8SiO_2$-S62 (**A**), $8SiO_2$-MMA194/$8SiO_2$-S205 (**B**), and $8SiO_2$-MMA350/$8SiO_2$-S360 (**C**) after 1 week of thermal annealing at $T$ = 140°C. Insets show AFM phase images of respective samples before thermal annealing. Scale bars, 1 μm. Short-chain brush system (A) is found to remain uniform after thermal annealing, whereas phase separation is observed in long-chain brush particle systems (B and C). Nonuniformity of preannealed state is observed for long-chain ligands [inset of (C)] indicating that phase separation commences during casting of films. The scheme illustrates the transition of interaction between brush particles with increasing degree of polymerization of tethered chains: hard sphere–type in case of short polymer chains [concentrated particle brush (CPB) regime] and polymer-like for long-chain systems [semidilute particle brush (SDPB) regime], see Discussion.

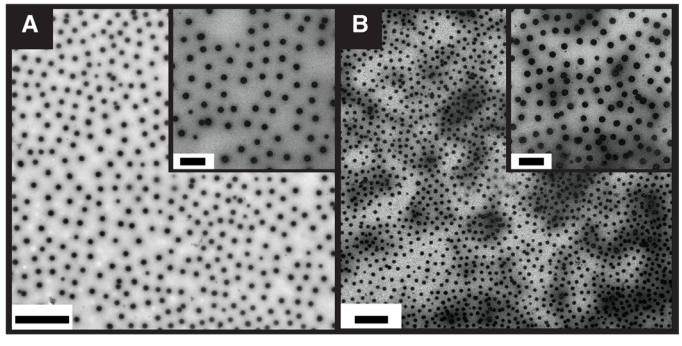


**Fig. 7. Ligand-induced phase separation in large particle blend system.** Bright-field TEM images of monolayer films of $60SiO_2$-MMA1470/$60SiO_2$-S1300 (50:50) blends in the presence of 15% DMP revealing SD-type phase separation. (**A**) As-cast film. (**B**) After $t$ = 24 hours of thermal annealing at $T$ = 140°C. Dark phase corresponds to PS ($RuO_4$ stain). Insets show magnified image. Scale bars, 500 nm (main figure) and 200 nm (insets).

of reversible mixing and phase separation of particle brush blends, we analyzed the structure evolution in the binary system $8SiO_2$-MMA257/$8SiO_2$-SAN262. To accelerate phase separation, we added a small amount (10 wt %) of DMP to the system. This system was chosen because of its similar molecular characteristics to the $8SiO_2$-MMA194/$8SiO_2$-S205 UCST system and the suitable lineup of thermal transitions (that is, LCST ≈ 160°C > $T_g$ ≈ 75°C > 25°C) that enables the vitrification of blend microstructures for structural characterization (note that the $T_g$ is lowered from approximately 115° to 75°C by DMP addition). Here, it is assumed that the LCST of the $8SiO_2$-PMMA/$8SiO_2$-PSAN particle brush blends is ≈160°C, equal to the LCST of corresponding linear PMMA/PSAN blends. To evaluate structure evolution during heating/cooling through LCST, we sequentially annealed particle brush blend films with thickness of ≈50 nm at 130°C (24 hours), 170°C (24 hours), and 130°/110°C (48 hours). The phase-separated microstructures were probed using TEM after 24-hour annealing steps. Figure 8 illustrates the thermal processing history and the structure evolution of the $8SiO_2$-MMA257/$8SiO_2$-SAN262 blend system during sequential annealing cycles.

Films in the preannealed state exhibited a weakly phase-separated structure similar to UCST blends (not shown here). This can be rationalized by considering Hildebrand solubility parameters ($\delta_{THF}$ = 18.6 $MPa^{1/2}$, $\delta_{PMMA}$ = 19.0 $MPa^{1/2}$, $\delta_{PSAN}$ = 19.6 $MPa^{1/2}$, and $\delta_{DMP}$ = 21.9 $MPa^{1/2}$) (*31*). The weak affinity of the solvent (THF) toward PMMA alters the thermodynamics of mixing and possibly results in partial phase separation during casting of films (*31*). Annealing of films for 24 hours at $T$ = 130°C resulted in completely homogeneous microstructures (see Fig. 8B). The dissolution of the partially phase-separated structure is expected because LCST is >130°C. It confirms the miscibility of the blend and also that the addition of DMP does not significantly alter the expected LCST characteristics (*32*). Subsequent annealing at $T$ = 170°C for 24 hours resulted in the formation of a bicontinuous morphology (Fig. 8C) with a characteristic correlation length of $d$ = 325 nm (determined by line intersection method from electron micrographs). The latter is consistent with a spinodal-type phase separation for a blend with near critical composition at $T$ > LCST (*22*). Subsequent annealing of phase-separated films at $T$ = 110° and 130°C resulted in the progressive decrease of $d$ along with the reduction of the contrast between adjacent domains (see Fig. 8, D and E), indicating the gradual "dissolution" of domains. The reduction of domain size was more pronounced when annealed at 110°C (see Fig. 8A)—this is interpreted as a consequence of the more negative interaction or "χ" parameter at lower $T$ that raised the thermodynamic driving force for mixing. In summary, the results displayed in Fig. 8 confirm LCST behavior of the $8SiO_2$-MMA257/$8SiO_2$-SAN262 system and correlate well with the expected behavior of linear PMMA/PSAN blends with LCST ≈160°C (*29*).

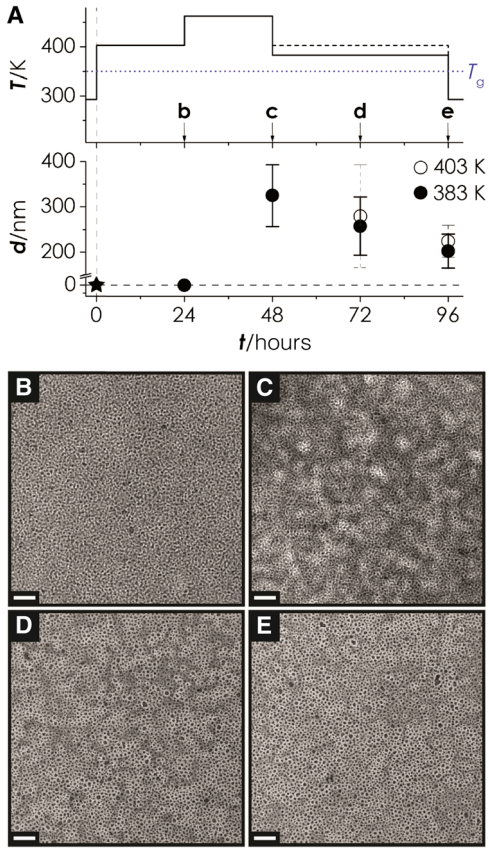


**Fig. 8. Reversible structure evolution in $8SiO_2$-MMA257/$8SiO_2$-SAN262 (50:50) LCST system.** Ten percent of DMP was added to accelerate kinetics. (**A**) Illustration of thermal processing steps: annealing at 403 K (130°C) for 24 hours; 443 K (170°C) for 24 hours; and 383 K/403 K (110°C/130°C) for 48 hours along with corresponding domain size $d$ (see text for more detail). The star symbol corresponds to preannealed state, filled black circles represent annealing states of which microstructures are presented. The dotted blue line at $T$ ~ 351 K (75°C) indicates the $T_g$ of the blend in the presence of DMP. TEM images depict film microstructures after subsequent annealing steps ($RuO_4$ stain of PSAN component). (**B**) Twenty-four hours of annealing at 403 K (130°C). (**C**) Twenty-four hours of annealing at 443 K (170°C). (**D**) Twenty-four hours of annealing at 383 K (110°C). (**E**) Forty-eight hours of annealing at 383 K (110°C). Scale bars, 200 nm. The micrographs reveal a transition from uniformly mixed structure (B) to bicontinuous phase-separated structure (C) after annealing at $T$ > LCST. Subsequent annealing at $T$ < LCST results in progressive reduction of domain size (D and E).

## DISCUSSION

Our results demonstrate that the interaction between polymeric ligands with distinct composition can drive UCST- or LCST-type phase separation processes in mixed particle brush systems in a similar way to the corresponding linear polymer blends. However, although the general trends are similar, the data also bring out several pertinent features that point to a more complex parameter space governing phase separation in particle brush blends that will be discussed in the following. The first feature is the existence of a threshold degree of polymerization to enable phase separation that exceeds the corresponding value for linear polymer blends. The latter is demonstrated by the $8SiO_2$-MMA68/$8SiO_2$-S62 system that remains miscible (see Fig. 6A) despite its degree of segregation $\chi\langle N\rangle \approx 2.43$ that exceeds the critical value "2" for phase separation in the corresponding linear polymer blend ($\chi\langle N\rangle$ is calculated assuming $\chi$ = 0.037 at $T$ = 140°C and an average degree of polymerization $\langle N\rangle$ = 65 for polymeric tethers). The second feature is a reduced scaling coefficient of domain growth and a significantly smaller domain size, as compared to those of linear polymer blends for analogous annealing conditions.

To gain insight into the role of the degree of polymerization $N$ of tethered chains in the phase separation process in particle brush blends, we first consider the effect of chain conformation on the interaction between polymer-tethered particles. It has been shown that the geometric constraints on chains that are tethered to a curved interface give rise to two-chain conformational regimes: in the vicinity

of the particle core (that is, in the limit of small $N$), the concentrated brush regime (CPB) is observed in which chains assume stretched chain conformations (experimental studies on particle brush melts suggest $h_{CPB} \sim N_{CPB}^{0.8}$, where $h_{CPB}$ denotes the brush height). In contrast, for sufficiently large $N$, the semidilute brush regime (SDPB) is observed that is characterized by relaxed chain conformations ($h_{SDPB} \sim N_{SDPB}^{0.5}$) (*16*, *31*, *33*). An approximate model to predict the transition between CPB and SDPB regimes was introduced by Tsuji and co-workers (*33*) and Ohno and co-workers (*34*), who extended the Daoud-Cotton model for star polymer systems to derive a "critical distance" that marks the CPB/SDPB transition. Applied to the "small" $SiO_2$ particles ($R_0$ = 7.7 nm) used in the present study, the model suggests the CPB/SDPB transition to occur at a critical degree of polymerization $N_{crit.} \approx 250$ (*16*). Thus, the analysis reveals that both $8SiO_2$-MMA68 and $8SiO_2$-S62 particle systems are in the "stretched" chain regime, whereas other particle systems are in the SDPB—this conclusion is also consistent with the analysis of the particle brush height using electron micrographs of particle monolayers (not shown here). The apparent miscibility of the $8SiO_2$-MMA68/$8SiO_2$-S62 blend system (see Fig. 6A) can then be rationalized as the consequence of two major contributing factors that reduce the thermodynamic driving force of phase separation. First, the dense packing of chains in CPB brush particles hinders brush interdigitation and hence reduces the number of segmental contacts between chemically distinct chains. This is supported by light scattering experiments on solutions of brush particles that revealed CPB particle brushes to interact via hard sphere–type potentials (*13*). It is also consistent with the results of previous studies on the structure and interactions of brush particles in polymer melts. These studies have shown that "dense ligand layers" are rather impenetrable to melt polymer chains of similar molecular size (*35*, *36*). The reduced number of contacts between chemically distinct chains decreases the specific energy gain upon phase separation and hence the (chemical) potential gradient that drives the separation process. However, whereas in the case of particle brush/polymer blends the presence of a mobile phase (that is, the melt) provides a kinetic path for phase separation even in weakly phase-separating systems, we hypothesize that the absence of a mobile phase in conjunction with the reduced driving force "freezes" CPB blends in the mixed state (*37*). In this context, it is interesting to note that contact angle measurements revealed a significant decrease of the surface energy of particle brush films as compared to linear homopolymer analogs (that is, $\gamma_{8SiO2\text{-}MMA194} \approx 26$ mJ/m$^2$, $\gamma_{8SiO2\text{-}S205} \approx 33$ mJ/m$^2$, $\gamma_{PMMA} \approx 41$ mJ/m$^2$, and $\gamma_{PS} \approx 40$ mJ/m$^2$). Although the origin of this decrease of surface tension in the case of particle brush films remains unresolved (we hypothesize it to be related to a more pronounced contribution of end groups in conjunction with fewer segmental contacts due to the repulsion between brushes), the similarity of surface tension between brush particles with distinct composition is an indicator for the reduced driving force of phase separation in CPB blend systems.

A further contribution to the reduction of the driving force of phase separation stems from the smaller number density of segment contacts due to the presence of particle cores. For example, assuming complete brush interdigitation, the cumulative pairwise interactions between ligands in brush particles will be reduced approximately by a factor of $(1 - \phi)$ as compared to the analogous linear polymer blend (with $\phi$ denoting the inorganic volume fraction). Because $\phi$ is large for CPB particles ($\phi > 0.3$), this "dilution effect" is more pronounced for CPB particle systems, whereas for SDPB systems, the inorganic content is comparatively small (see Table 1).

A second interesting observation pertains to the kinetics of domain growth in the $8SiO_2$-MMA194/$8SiO_2$-S205 (50:50) blend system (shown in Fig. 5) that scales with time as $d \sim t^{0.22}$, which is significantly less than the expected value of $^1/_3$ for diffusion-controlled domain coarsening (*38*). Scaling coefficients less than $^1/_3$ were reported for thin film polymer blends in the literature and have been rationalized as a consequence of geometric constraints that limit domain coarsening when the domain size becomes comparable to the thickness of films (*29*). Here, we want to point to an additional distinguishing feature between particle brush and linear polymer blends that could contribute to a reduction of the scaling coefficient. In principle, phase separation by SD is initiated by the spontaneous growth of composition fluctuations as the system is being quenched into the unstable region of the phase diagram. Three stages of domain growth are distinguished. During the first stage of phase separation, the amplitude of fluctuations increases, yet their wavelength remains constant. This is followed by a diffusion-controlled intermediate stage, during which both composition and domain size change ($d \sim t^{1/3}$), and a final hydrodynamic-driven stage where only domain size increases ($d \sim t$) (*39*). The characteristic spinodal wavelength is typically of the order of the size of the constituent polymer chains and can be influenced by the quench depth and composition of the system (*40*). Given the limited (time) resolution of our experiments, the first stage of phase separation could not be observed in our study. However, literature reports on the phase separation in star polymer systems have shown that the spinodal wavelength of star and linear polymers is approximately equal (*41*). Therefore, we hypothesize that the spinodal wavelength in brush particle blends is similar to star and linear polymer blend analogs. Note that this implies the spinodal wavelength in particle brush materials to be less than the size of individual brush particles—a constraint that could alter domain growth. For example, de Gennes (*42*) analyzed the kinetics of SD under the constraint that the spinodal wavelength is less than the distance between entanglement points and concluded normal diffusional growth to be preceded by an "anomalous growth regime" during which growth occurs by local reorganization rather than diffusion. The scaling coefficient for this "anomalous growth regime" was predicted to be $^1/_5$, close to the experimental value of 0.22. To further elucidate the role of brush architecture on the structure evolution in phase-separating particle brush blends would be an interesting subject for future research.

Finally, we want to comment on the domain size in phase-separated particle brush blends that is substantially smaller (by about one order of magnitude) than values reported for linear polymer blends (*20*). To illustrate this point, we note that a reference system composed of a symmetric blend of PS/PMMA homopolymers with degree of polymerization $N_{PMMA}$ = 204 and $N_{PS}$ = 216 (comparable to PS/PMMA tethers in the $8SiO_2$-MMA194/$8SiO_2$-S205 system shown in Figs. 3 and 4) did show final-stage separation after annealing for 24 hours at $T$ = 140°C (see fig. S1). We rationalize the small domain size in particle brush blends as a consequence of the combination of the reduced thermodynamic driving force (see discussion above) and the reduced diffusion kinetics. The latter can be appreciated by comparison with the topologically related system of star polymers, for which dynamical properties have been extensively studied. For example, Klein and co-workers (*43*) proposed that the self-diffusion coefficient in star polymer melts depends on the degree of polymerization of branch chains ($N_b$) and the number of chains ($f$) as $D(N_b, f) \sim \exp[-CN_b(f\text{-}2)]$, where $C$ is a constant. Given that the number of graft chains for 15-nm particles is ≈350 (assuming a

grafting density of σ = 0.5 $nm^{-2}$), the particle brush mobility is expected to be significantly reduced as compared to linear polymer systems. For practical purposes, this reduction in diffusional kinetics might be balanced by the addition of small molecular additives that raise molecular mobility as demonstrated for the case of $60SiO_2$-MMA1470/$60SiO_2$-S1300 (see Fig. 7). Hence, the reduced separation kinetics does not preclude the concept of "ligand-induced phase separation" to be applied to larger particle systems. Finally, we note that the exponential decrease of $D$ with $N_b$ also suggests the existence of an "optimum" $N$ for maximizing domain growth that is determined by the balance of thermodynamic driving force and diffusivity. The increased domain size in case of the intermediate $8SiO_2$-MMA194/$8SiO_2$-S205 system confirms this proposition, although the currently available data do not allow for a more quantitative analysis.

## CONCLUSION

Ligand interactions in blends of polymer-tethered nanoparticles can impart UCST- and LCST-type phase behavior on particle mixtures similar to the phase behavior of the respective linear polymer blends. Cooling (or heating) of particle brush blends with appropriate architecture below (or above) the UCST (or LCST) thus results in the formation of monoparticle domain structures with characteristic size and shape that can be tuned by variation of the composition and thermal annealing conditions. The ability to autonomously organize multicomponent particle mixtures into monotype microdomain structures of controlled size and shape by harnessing phase separation processes could enable transformative advances in the high-throughput fabrication of microstructured particle solid films. The latter play an important role in a wide range of particle-enabled material technologies, for example, photovoltaics or nano-enabled solid-state lighting technologies. Furthermore, the reversible formation and dissolution of microstructures in multicomponent particle solids by thermal cycling of LCST particle brush blends through the critical temperature could enable important advances in the development of smart and adaptive coating technologies. To facilitate these advances, a better understanding of the governing parameters that control the structure evolution in particle brush blends should be accomplished. In particular, although the structure evolution is consistent with phase separation by NG or SD, the kinetics of structure evolution shows distinctive differences (such as a reduced scaling coefficient) as compared to linear blends. Given the complex parameter space in polymer-tethered particles, this might also provide opportunities to gain novel physical insights into the role of geometric constraints in phase separation in polymer systems.

## MATERIALS AND METHODS

### Particle brush synthesis

The synthesis of polymer-tethered particles was performed using SI-ATRP according to the previously published procedures (*24*–*26*). In a typical synthetic procedure, silica nanoparticles were bound with the initiator by using 5-hexen-1-ol, α-bromoisobutyryl bromide, and triethoxysilane to synthesize a tetherable ATRP initiator 6-(triethoxysilyl) hexyl α-bromoisobutyrate. For the polymerization, a mixture of initiator-modified silica nanoparticles ($SiO_2$-Br) and anisole was stirred in a Schlenk flask for 24 hours to form a homogeneous suspension. Subsequently, styrene, *N*,*N*′,*N*″,*N*″-pentamethyldiethylenetriamine (PMDETA), and $CuBr_2$ were added to the flask with a rare earth magnetic stir bar. The use of a sufficiently strong stir bar was required to prohibit vitrification that could occur, especially at high monomer conversion. The solution underwent three freeze-pump-thaw cycles before being immersed in liquid nitrogen and then purged with nitrogen. Then, CuBr was added to the flask. The flask was sealed with a glass stopper and evacuated before being back-refilled with nitrogen three times. The reaction mixture was then warmed to room temperature and placed in an oil bath heated to 70°C to initiate polymerization. The final molar ratios of reaction components in a typical reaction were approximately $[Styrene]_0/[SiO_2\text{-}Br]_0/[CuBr]_0/[CuBr_2]_0/[PMDETA]_0$ of 2000:1:2.5:0.25:2.75 with a volume fraction of nonreactive solvents of 5.4% dimethylformamide and 40% anisole in a 100-ml flask and stirred at approximately 1000 rpm. The polymerization was stopped by exposing the catalyst to oxygenated THF after cooling under continuous stirring. The final product was dialyzed against THF and methanol until the copper(II) catalyst was removed as evidenced by disappearance of its characteristic color.

Styrene (Aldrich, 99%) was purified by passing through a basic alumina column before use. Copper(I) bromide was prepared by reduction of an aqueous solution of $CuBr_2$ with an aqueous solution of ascorbic acid, and copper(I) chloride was prepared by reduction of a $CuCl_2$ aqueous solution using an aqueous solution of sodium sulfite. Both copper halides were then sequentially filtered, washed with methanol, dried, and stored under vacuum before use. Silica nanoparticles ($SiO_2$NP), 30% solution in isopropanol, were donated by Nissan Chemical Corporation and used as received. 5-Hexen-1-ol (98%), α-bromoisobutyryl bromide (98%), triethoxysilane (95%), ethyl α-bromoisobutyrate (98%), 4,4′-dinonyl-2,2′-bipyridine (dNbpy, 99%), PMDETA (99%), and anisole (99%) were purchased from Aldrich and used as received. All other chemicals and solvents were supplied by Aldrich and Acros Organics.

### Debromination procedure

The debromination was performed under an atmosphere of nitrogen. In a typical procedure, the as-prepared $SiO_2$-PMMA*N*, $SiO_2$-PMMA*N*, or $SiO_2$-PSA*NN* brush particles (0.03 mmol Br) and *N*,*N*′-dimethylformamide (10 ml) were stirred in a Schlenk flask for 2 hours to form a homogeneous solution. Subsequently, thiophene (0.3 mmol) and triethylamine (0.3 mmol) were added slowly to the flask under vigorous stirring. The flask was sealed with a glass stopper and evacuated before being back-refilled with nitrogen. The reaction mixture was immersed in an oil bath at 45°C overnight. The product was precipitated by adding the reaction mixture to methanol, and the solid was filtered and washed with methanol before drying in a vacuum oven at 60°C.

### Characterization

Inorganic content of particle brushes and decomposition characteristics were made using weight fractions measured from thermogravimetric analysis (TGA) on a Q50 TGA analyzer from TA Instruments under nitrogen up to 850°C at a scan rate of 20°C/min. To study decomposition, we held temperature at a selected value (that is, 250°C) for a period of time and slowed the scan period (5°C /min) to accurately assess weight loss before continued scanning at the normal rate.

Molecular weight and dispersity were measured by GPC using a Waters 515 pump and Waters 2414 differential refractometer (λ = 930 nm) and a Wyatt Technology DAWN EOS multiangle laser light scattering detector using PSS columns (Styrogel $10^5$, $10^3$, and $10^2$ Å) for PS and Waters Microstyragel columns (guard, $10^2$, $10^3$, and $10^5$ Å)

in THF as an eluent (35°C, flow rate of 1 ml/min) with toluene and diphenyl ether used as internal references. Linear PS or PMMA standard was used for calibration. Chains were cleaved from particles by etching of particles in hydrofluoric acid (HF) in a polypropylene vial for 20 hours, neutralized with ammonium hydroxide, and dried with magnesium sulfate before running GPC. Hydrofluoric acid (50 volume % HF) was purchased from Acros Organics and used as received. THF was purchased from Aldrich and used as received.

### Atomic force microscopy

Blended films of PMMA@$SiO_2$ and PS@$SiO_2$ were prepared by spin coating concentrated solutions (~35 mg/ml) of particle brushes in toluene onto silicon substrates with their native oxide layer intact that were cleaned with acetone, isopropanol, and deionized water immediately before coating at 2000 rpm for 30 s. When annealing, temperature changes were introduced very rapidly (<5 min) relative to the annealing times, such that the effect of the heating and cooling periods on structural evolution can be ignored. Vacuum-annealed and not annealed samples were imaged for both height and phase using an NT-MDT SolverNEXT system in tapping mode under atmospheric conditions at scan sizes of 5 μm × 5 μm or smaller to reasonably discern phase-separated domains using a silicon cantilever (force constant, 40 N $m^{-1}$; resonance frequency, 300 kHz; tip radius, <10 nm). Film thickness was measured by scratching the film off and measuring the height change between the substrate and film surface.

### Transmission electron microscopy

Multilayer films were made by spin coating concentrated solutions (≈35 mg/ml) of particle brushes onto PAA films (PAA was obtained as a 25 wt % solution in water from Sigma-Aldrich). Particle brush films were lifted off from the substrate by water immersion and subsequently transferred onto copper grids for analysis. The thickness of the films was approximately 110 to 140 nm as measured by a line scratch test with AFM.

## SUPPLEMENTARY MATERIALS

Supplementary material for this article is available at http://advances.sciencemag.org/cgi/content/full/2/12/e1601484/DC1

fig. S1. Phase separation in PS/PMMA polymer blend.

## REFERENCES AND NOTES


1. T. W. Odom, M.-P. Pileni, Nanoscience. *Acc. Chem. Res.* **41**, 1565 (2008).
2. D. V. Talapin, J.-S. Lee, M. V. Kovalenko, E. V. Shevchenko, Prospects of colloidal nanocrystals for electronic and optoelectronic applications. *Chem. Rev.* **110**, 389–458 (2010).
3. L. Mazzola, Commercializing nanotechnology. *Nat. Biotechnol.* **21**, 1137–1143 (2003).
4. K. J. M. Bishop, C. E. Wilmer, S. Soh, B. A. Grzybowski, Nanoscale forces and their uses in self-assembly. *Small* **5**, 1600–1630 (2009).
5. S. Ojha, B. Beppler, H. Dong, K. Matyjaszewski, S. Garoff, M. R. Bockstaller, Impact of polymer graft characteristics and evaporation rate on the formation of 2-D nanoparticle assemblies. *Langmuir* **26**, 13210–13215 (2010).
6. M. A. Boles, M. Engel, D. V. Talapin, Self-assembly of colloidal nanocrystals: From intricate structures to functional materials. *Chem. Rev.* **116**, 11220–11289 (2016).
7. Y. Min, M. Akbulut, K. Kristiansen, Y. Golan, J. Israelachvili, The role of interparticle and external forces in nanoparticle assembly. *Nat. Mater.* **7**, 527–538 (2008).
8. C. B. Murray, C. R. Kagan, M. G. Bawendi, Synthesis and characterization of monodisperse nanocrystals and close-packed nanocrystal assemblies. *Annu. Rev. Mater. Sci.* **30**, 545–610 (2000).
9. E. V. Shevchenko, D. V. Talapin, N. A. Kotov, S. O'Brien, C. B. Murray, Structural diversity in binary nanoparticle superlattices. *Nature* **439**, 55–59 (2009).
10. P. Cigler, A. K. R. Lytton-Jean, D. G. Anderson, M. G. Finn, S. Y. Park, DNA-controlled assembly of a NaTl lattice structure from gold nanoparticles and protein nanoparticles. *Nat. Mater.* **9**, 918–922 (2010).
11. C. A. Mirkin, R. L. Letsinger, R. C. Mucic, J. J. Storhoff, A DNA-based method for rationally assembling nanoparticles into macroscopic materials. *Nature* **382**, 607–609 (1996).
12. C. M. Hui, J. Pietrasik, M. Schmitt, C. Mahoney, J. Choi, M. R. Bockstaller, K. Matyjaszewski, Surface-initiated polymerization as an enabling tool for multifunctional (nano-) engineered hybrid materials. *Chem. Mater.* **26**, 745–762 (2014).
13. P. Voudouris, J. Choi, H. Dong, M. R. Bockstaller, K. Matyjaszewski, G. Fytas, Effect of shell architecture on the static and dynamic properties of polymer-coated particles in solution. *Macromolecules* **42**, 2721–2728 (2009).
14. J. Choi, C. M. Hui, J. Pietrasik, H. Dong, K. Matyjaszewski, M. R. Bockstaller, Toughening fragile matter: Mechanical properties of particle solids assembled from polymer-grafted hybrid particles synthesized by ATRP. *Soft Matter* **8**, 4072–4082 (2012).
15. J. Choi, H. Dong, K. Matyjaszewski, M. R. Bockstaller, Flexible particle array structures by controlling polymer graft architecture. *J. Am. Chem. Soc.* **132**, 12537–12539 (2010).
16. M. Schmitt, J. Choi, C. M. Hui, B. Chen, E. Korkmaz, J. Yan, S. Margel, O. B. Ozdoganlar, K. Matyjaszewski, M. R. Bockstaller, Processing fragile matter: Effect of polymer graft modification on the mechanical properties and processibility of (nano-) particulate solids. *Soft Matter* **12**, 3527–3537 (2016).
17. E. Alonso-Redondo, M. Schmitt, Z. Urbach, C. M. Hui, R. Sainidou, P. Rembert, K. Matyjaszewski, M. R. Bockstaller, G. Fytas, A new class of tunable hypersonic phononic crystals based on polymer-tethered colloids. *Nat. Commun.* **6**, 8309 (2015).
18. C. A Grabowski, H. Koerner, J. S. Meth, A. Dang, C. M. Hui, K. Matyjaszewski, M. R. Bockstaller, M. F. Durstock, R. A. Vaia, Performance of dielectric nanocomposites: Matrix-free, hairy nanoparticle assemblies and amorphous polymer–nanoparticle blends. *ACS Appl. Mater. Interfaces* **6**, 21500–21509 (2014).
19. M. N. Tchoul, S. P. Fillery, H. Koerner, L. F. Drummy, F. T. Oyerokun, P. A. Mirau, M. F. Durstock, R. A. Vaia, Assemblies of titanium dioxide-polystyrene hybrid nanoparticles for dielectric applications. *Chem. Mater.* **22**, 1749–1759 (2010).
20. D. U. Ahn, Z. Wang, I. P. Campbell, M. P. Stoykovich, Y. Ding, Morphological evolution of thin PS/PMMA films: Effects of surface energy and blend composition. *Polymer* **53**, 4187–4191 (2012).
21. T. P. Russell, R. P. Hjelm Jr., P. A. Seeger, Temperature dependence of the interaction parameter of polystyrene and poly(methyl methacrylate). *Macromolecules* **23**, 890–893 (1990).
22. D. R. Paul, J. W. Barlow, A binary interaction model for miscibility of copolymers in blends. *Polymer* **25**, 487–494 (1984).
23. M. Suess, J. Kressler, H. W. Kammer, The miscibility window of poly(methyl methacrylate)/poly(styrene-*co*-acrylonitrile) blends. *Polymer* **28**, 957–960 (1987).
24. G. Wen, Z. Sun, T. Shi, J. Yang, W. Jiang, L. An, B. Li, Thermodynamics of PMMA/SAN blends: Application of the Sanchez–Lacombe lattice fluid theory. *Macromolecules* **34**, 6291–6296 (2001).
25. K. Matyjaszewski, N. V. Tsarevsky, Nanostructured functional materials prepared by atom transfer radical polymerization. *Nat. Chem.* **1**, 276–288 (2009).
26. J. Pyun, K. Matyjaszewski, Synthesis of nanocomposite organic/inorganic hybrid materials using controlled/"living" radical polymerization. *Chem. Mater.* **13**, 3436–3448 (2001).
27. L. Bombalski, H. Dong, J. Listak, K. Matyjaszewsk, M. R. Bockstaller, Null-scattering hybrid particles using controlled radical polymerization. *Adv. Mater.* **19**, 4486–4490 (2007).
28. A. Karim, T. M. Slawecki, S. K. Kumar, J. F. Douglas, S. K. Satija, C. C. Han, T. P. Russell, Y. Liu, R. Overney, J. Sokolov, M. H. Rafailovich, Phase-separation-induced surface patterns in thin polymer blend films. *Macromolecules* **31**, 857–862 (1998).
29. H.-j. Chung, R. J. Composto, Breakdown of dynamic scaling in thin film binary liquids undergoing phase separation. *Phys. Rev. Lett.* **92**, 185704 (2004).
30. M. Harris, G. Appel, H. Ade, Surface morphology of annealed polystyrene and poly(methyl methacrylate) thin film blends and bilayers. *Macromolecules* **36**, 3307–3314 (2003).
31. D. M. Koenhen, C. M. Smolders, The determination of solubility parameters of solvents and polymers by means of correlations with other physical quantities. *J. Appl. Polym. Sci.* **19**, 1163–1179 (1975).
32. B. D. Ermi, A. Karim, J. Douglas, Formation and dissolution of phase-separated structures in ultrathin blend films. *J. Polym. Sci. Part B Polym. Phys.* **36**, 191–200 (1998).
33. Y. Tsuji, K. Ohno, S. Yamamoto, A. Goto, T. Fukuda, Structure and properties of high-density polymer brushes prepared by surface-initiated living radical polymerization. *Adv. Polym. Sci.* **197**, 1–45 (2006).
34. K. Ohno, T. Morinaga, S. Takeno, Y. Tsukii, T. Fukuda, Suspensions of silica particles grafted with concentrated polymer brush: Effects of graft chain length on brush layer thickness and colloidal crystallization. *Macromolecules* **40**, 9143–9150 (2007).
35. S. K. Kumar, R. Krishnamoorti, Nanocomposites: Structure, phase behavior, and properties. *Annu. Rev. Chem. Biomol. Eng.* **1**, 37–58 (2010).
36. I. Borukhov, L. Leibler, Enthalpic stabilization of brush-coated particles in a polymer melt. *Macromolecules* **35**, 5171–5182 (2002).
37. S. K. Kumar, N. Jouault, B. Benicewicz, T. Neely, Nanocomposites with polymer grafted nanoparticles. *Macromolecules* **46**, 3199–3214 (2013).

38. A. Z. Akcasu, R. Klein, A nonlinear theory of transients following step temperature changes in polymer blends. *Macromolecules* **26**, 1429–1441 (1993).
39. C. C. Lin, H. S. Jeon, N. P. Balsara, B. Hammouda, Spinodal decomposition in multicomponent polymer blends. *J. Chem. Phys.* **103**, 1957–1971 (1995).
40. P. Pincus, Dynamics of fluctuations and spinodal decomposition in polymer blends. II. *J. Chem. Phys.* **75**, 1996–2000 (1981).
41. B. J. Factor, T. P. Russell, B. A. Smith, L. J. Fetters, B. J. Bauer, C. C. Han, Phase-separation kinetics in mixtures of linear and star-shaped polymers. *Macromolecules* **23**, 4452–4455 (1990).
42. P. G. de Gennes, Dynamics of fluctuations and spinodal decomposition in polymer blends. *J. Chem. Phys.* **72**, 4756–4763 (1980).
43. J. Klein, D. Fletcher, L. J. Fetters, Diffusional behaviour of entangled star polymers. *Nature* **304**, 526–527 (1983).

**Acknowledgments**
**Funding:** M.R.B., R.F.D., K.M., and A.K. acknowledge financial support by the NSF (via DMR-1410845, DMR-1501324, and DMR-1411046) and the Department of Energy (via DE-EE0006702). M.S. further acknowledges financial support from the John and Clare Bertucci Graduate Fellowship. J.Z. acknowledges scholarship support by the China Scholarship Council and by the Scott Institute for Energy Innovation at Carnegie Mellon University. The authors further acknowledge use of the Materials Characterization Facility at Carnegie Mellon University supported by grant MCF-677785. **Author contributions:** M.S., J.L., and X.N. performed characterization experiments. J.Z. performed materials synthesis. M.R.B. conceived the project and supervised the material characterization. K.M. supervised the material synthesis. A.K. and R.Z. performed surface energy measurements and assisted in the interpretation of results. All authors have discussed the results and commented on the manuscript. **Competing interests:** The authors declare that they have no competing interests. **Data and materials availability:** All data needed to evaluate the conclusions in the paper are present in the paper and/or the Supplementary Materials. Additional data related to this paper may be requested from M.R.B. Samples and characterization data are archived and can be made available upon request.

Submitted 29 June 2016
Accepted 11 November 2016
Published 23 December 2016
10.1126/sciadv.1601484

**Citation:** M. Schmitt, J. Zhang, J. Lee, B. Lee, X. Ning, R. Zhang, A. Karim, R. F. Davis, K. Matyjaszewski, M. R. Bockstaller, Polymer ligand–induced autonomous sorting and reversible phase separation in binary particle blends. *Sci. Adv.* **2**, e1601484 (2016).

ScienceAdvances

# Polymer ligand–induced autonomous sorting and reversible phase separation in binary particle blends

Michael Schmitt, Jianan Zhang, Jaejun Lee, Bongjoon Lee, Xin Ning, Ren Zhang, Alamgir Karim, Robert F. Davis, Krzysztof Matyjaszewski and Michael R. Bockstaller

*Sci Adv* **2** (12), e1601484.
DOI: 10.1126/sciadv.1601484